

# A dynamical magnetosphere model for periodic $H\alpha$ emission from the slowly rotating magnetic O star HD 191612

Jon O. Sundqvist<sup>1\*</sup>, Asif ud-Doula<sup>2</sup>, Stanley P. Owocki<sup>1</sup>, Richard H. D. Townsend<sup>3</sup>  
Ian D. Howarth<sup>4</sup>, Gregg A. Wade<sup>5</sup>, and the MiMeS Collaboration

<sup>1</sup>University of Delaware, Bartol Research Institute, Newark, Delaware 19716, USA

<sup>2</sup>Penn State Worthington Scranton, 120 Ridge View Drive, Dunmore, PA 18512, USA

<sup>3</sup>University of Wisconsin, Department of Astronomy, Madison, WI 53706, USA

<sup>4</sup>University College London, Department of Physics and Astronomy, Gower Place, London WC1E 6BT, United Kingdom

<sup>5</sup>Royal Military College of Canada, Department of Physics, PO Box 17000 Kingston, Ontario K7K 7B4, Canada

Accepted 2012-02-28. Received 2011-12-11

## ABSTRACT

The magnetic O-star HD 191612 exhibits strongly variable, cyclic Balmer line emission on a 538-day period. We show here that its variable  $H\alpha$  emission can be well reproduced by the rotational phase variation of synthetic spectra computed directly from full radiation magneto-hydrodynamical simulations of a magnetically confined wind. In slow rotators such as HD 191612, wind material on closed magnetic field loops falls back to the star, but the transient suspension of material within the loops leads to a statistically overdense, low velocity region around the magnetic equator, causing the spectral variations. We contrast such “dynamical magnetospheres” (DMs) with the more steady-state “centrifugal magnetospheres” of stars with rapid rotation, and discuss the prospects of using this DM paradigm to explain periodic line emission from also other non-rapidly rotating magnetic massive stars.

**Key words:** stars: winds, outflows - stars: magnetic field - stars: rotation - MHD

## 1 INTRODUCTION

Shortly after Donati et al. (2006) detected a strong magnetic field in the Galactic Of?p star HD 191612, Howarth et al. (2007) demonstrated that the variable equivalent widths of its optical Balmer and HeI lines (e.g., Walborn et al. 2003) can be accurately phased according to a 538-day period, where in particular the outstanding  $H\alpha$  variation shows strict periodicity. Since this period is unrelated to the much longer orbital period  $P_{\text{orb}} = 1542$  d of HD 191612 and its binary companion (Howarth et al. 2007), rotational modulation of a magnetically confined wind seems the most likely origin for the variability, as already suggested by Donati et al. (2006). But in contrast to centrifugally supported magnetosphere models, which have been successfully applied to Balmer line variability in rapid rotators such as the B star  $\sigma$  Ori E (Townsend et al. 2005), it is not clear how a very slow rotator such as HD 191612 can sustain a magnetosphere

with sufficient accumulation of wind plasma to explain the strong and periodic Balmer emission.

To reproduce the  $H\alpha$  variation of HD 191612, Howarth et al. (2007) suggested two geometrical toy models. One of these was indeed inspired by the plasma distribution qualitatively expected from a magnetically confined wind; it is a tilted, limb-darkened, geometrically thin disc, where the sum of observer inclination  $i$  and obliquity  $\beta$  (the angle between the rotation and magnetic axes) must be  $i + \beta \approx 100^\circ$  for the  $H\alpha$  modulation to be fit.

Wade et al. (2011) recently analysed Stokes V spectra of HD 191612. Assuming a dipole oblique rotator, these authors derived  $i + \beta = 95 \pm 10^\circ$ , and by matching electron scattering modelling to the observed photometric variability further obtained  $i \geq 30^\circ$ . A tentative reference geometry  $i = 30^\circ$  and  $\beta = 67 \pm 5^\circ$  was then suggested from speculating that the orbital and spin angular momenta of HD 191612 be aligned, and a surface dipole (polar) field  $B_d = 2450 \pm 400$  G derived.

This Letter examines to what extent full radiation magneto-hydrodynamical (MHD) simulations of a magnet-

\* E-mail: jon@bartol.udel.edu

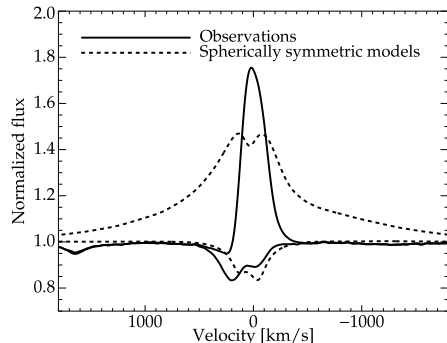


**Figure 1.** Observed (Howarth et al. 2007) and synthetic H $\alpha$  spectra during phases close to minimum and maximum. Synthetic FASTWIND spectra are computed for two different mass-loss rates under the assumption of spherical symmetry (see Sect. 2).

**Table 1.** Summary of stellar, wind, and magnetospheric parameters of HD 191612 (Howarth et al. 2007; Wade et al. 2011).

Name	Parameter	Value
Effective temperature	$T_{\text{eff}}$	$35\,000 \pm 1\,000$ K
Surface gravity	$\log g$	$3.5 \pm 0.1$
Stellar radius	$R_{\star}$	$14.5 R_{\odot}$
Helium abundance	$n_{\text{He}}/n_{\text{H}}$	0.1
Terminal speed	$v_{\infty}$	2700 km/s
Mass-loss rate and clumping factor	$\dot{M}\sqrt{f_{\text{cl}}}$	$1.6 \times 10^{-6} M_{\odot}/\text{yr}$
Surface polar magnetic field	$B_{\text{d}}$	$2450 \pm 400$ G
Obliquity and observer inclination	$\beta + i$	$95 \pm 10^{\circ}$

ically confined wind, along with detailed radiative transfer calculations, can actually reproduce HD 191612’s observed H $\alpha$  variability, under the wind, magnetic, and geometric constraints derived by Howarth et al. (2007) and Wade et al. (2011).

## 2 H $\alpha$ IN A SPHERICALLY SYMMETRIC WIND MODEL

To set the stage, we first compute synthetic H $\alpha$  profiles for two different mass-loss rates using the spherically symmetric, unified (photosphere+wind) NLTE (=Non Local Thermodynamic Equilibrium) model atmosphere code FASTWIND (Puls et al. 2005), taking stellar and wind parameters from Howarth et al. (2007) (Table 1). Fig. 1 confronts such models with the observed H $\alpha$  line profiles during minimum and maximum phases.

The model-fit during minimum phase is acceptable. Indeed, it is equivalent to that of Howarth et al. (2007), from which  $\dot{M}\sqrt{f_{\text{cl}}} = 1.6 \times 10^{-6} M_{\odot}/\text{yr}$  was derived for HD 191612. Here  $f_{\text{cl}} \equiv \frac{\langle \rho^2 \rangle}{\langle \rho \rangle^2} \geq 1$  is the wind clumping factor, with average mass density  $\langle \rho \rangle$ .  $f_{\text{cl}}$  enters the analysis because H $\alpha$  is a recombination based line in O stars, which means that its line strength is greater in a small-scale structured (‘clumped’) wind than in a smooth wind with the same mass-loss rate (e.g., Sundqvist et al. 2011).

In an attempt to also match the maximum phase, we next calculated a test-model with 5 times higher mass-loss rate. However, Fig. 1 clearly shows that this synthetic H $\alpha$  profile is much broader than the observed one. This indicates that the variable H $\alpha$  emission does not stem from a variable global mass-loss rate accompanied by a spherically symmetric velocity field such as the  $v = v_{\infty}(1 - 1/r)^{\beta}$  field assumed in FASTWIND, here with  $\beta = 1$ . Rather the variability might be caused by a confined region of wind material with high density and low velocity; such confinement may indeed stem from the strong magnetic field in HD 191612 channeling its radiatively driven wind outflow to form a stellar magnetosphere. We now describe our efforts to model this hypothesized structure.

## 3 SIMULATIONS

### 3.1 Modelling a dynamical magnetosphere

Following the general procedure outlined by ud-Doula & Owocki (2002), we compute a 2-D radiation MHD wind simulation of HD 191612, assuming a dipole magnetic field. Hydrodynamical variables are specified on a standard, right-handed spherical grid  $(r, \theta, \phi)$ , defined relative to a Cartesian set  $(x, y, z)$ , where we assume symmetry in  $\phi$ . The energy equation is treated as by Gagné et al. (2005) and the radiation line force is calculated within the Sobolev approximation using standard CAK (Castor et al. 1975) theory. Since the rotation of HD 191612 is extremely slow, the inferred period of 537.6 days (Howarth et al. 2007) implies an equatorial rotation speed  $v_{\text{rot}} = 1.4$  km/s, we may neglect rotational effects on the dynamics (and thus use the same simulation for any choice of obliquity  $\beta$ ).

The effectiveness of the magnetic field in channeling the stellar wind outflow may be characterized by the ratio of magnetic to wind kinetic energy density,

$$\eta \equiv \frac{B^2/8\pi}{\rho v^2/2} = \eta_{\star} \frac{(r/R_{\star})^{-4}}{v(r)/v_{\infty}}, \quad (1)$$

where the second equality defines the so-called ‘wind confinement parameter’  $\eta_{\star} \equiv B_{\star}^2 R_{\star}^2 / (\dot{M} v_{\infty})$  (ud-Doula & Owocki 2002), with  $B_{\star}$  the dipole equatorial surface field strength. If  $\eta_{\star} > 1$ , the dipole Alfvén radius  $R_{\text{A}} \approx \eta_{\star}^{1/4} R_{\star}$ , at which the magnetic and wind energy densities are equal, is located away from the stellar surface, allowing then for some wind material to be channeled along closed loops towards the magnetic equator (see Fig. 2). But the much steeper radial decline of the dipole magnetic energy density ( $\sim 1/r^6$ ) than the wind kinetic energy density ( $\sim 1/r^2$ ), means that at large enough radii the wind will always force the field lines to open up and essentially follow the radial wind flow.

The simulation here assumes strong confinement,  $\eta_{\star} = 50$ , in accordance with the magnetic field strength recently derived by Wade et al. (2011) and the wind parameters derived by Howarth et al. (2007), adopting  $f_{\text{cl}} = 1$ . It is well established that the winds of hot, massive O stars are indeed clumped (see Sundqvist et al. 2011, for a recent review). But a theoretical development of such stochastic, small-scale inhomogeneities, as caused by the strong instability inherent to line-driven winds (e.g., Owocki et al. 1988), requires a non-Sobolev treatment of the radiation line force, and has

yet to be implemented within any MHD simulation. However, in terms of the H $\alpha$  modelling that is the focus of this paper, we are still effectively modelling  $\dot{M}\sqrt{f_{\text{cl}}}$  (see Sect. 2), but simply neglecting any *dynamical* effects such stochastic, small-scale structures might have upon the large-scale wind structure imposed by the magnetic field.

The upper panels of Fig. 2 plot the density squared of two simulation snapshots. They illustrate how below  $r \approx R_A \approx 2.7R_*$ , the wind does indeed become trapped by the closed field-line loops, whereby the material is pulled back by gravity onto the star over a dynamical time-scale. But a key point here is that, despite the very dynamical behaviour, the transient suspension of material within such closed loops still results in a wind region, in the vicinity of the magnetic equator, that *statistically* is overdense (Fig. 2, lower-left panel). Further, as a result of the colliding wind material at individual loop tops, this overdense region is also characterized by very low velocities (Fig. 2, lower-right panel), in qualitative agreement with the narrowness of the observed H $\alpha$  emission discussed in Sect. 2.

The structures predicted by these simulations are physically distinct from those predicted for rapidly rotating magnetic stars with  $R_A > R_K$  (Townsend & Owocki 2005; Townsend et al. 2007; ud-Doula et al. 2008), where  $R_K = (v_{\text{rot}}/v_{\text{crit}})^{-2/3}R_*$  is the Kepler co-rotation radius for critical rotation speed  $v_{\text{crit}}$ . For such stars, the centrifugal forces can support any trapped material above  $R_K$ , allowing then the magnetically confined wind to accumulate material and form a *centrifugal magnetosphere* (CM). In contrast, the characteristic structure described above, appropriate for slowly rotating massive stars with  $R_K > R_A > R_*$ , instead establishes the concept of a *dynamical magnetosphere* (DM) (see also Petit et al. 2011).

In hot coronae from the sun and some magnetically active cool stars, there are analogous examples of regions of dynamical infall (“coronal rain”; e.g. Eibe et al. 1999) or centrifugally supported prominences (Collier Cameron et al. 2003; Jardine & van Ballegooijen 2005), fed largely by the transient eruptive propulsion of stellar flares. By contrast, hot-star magnetospheres are fed by the quasi-steady wind upflow driven by the star’s radiation, allowing for persistent Balmer emission that has been monitored over multi-year time-scales spanning many rotation periods.

Note that even rapid rotators will have a DM component at  $r \lesssim R_K$ . But the H $\alpha$  emission contribution from this part will be insignificant because of the much higher densities at  $R_K < r < R_A$  (see, e.g., Fig. 7 in Townsend et al. 2007). These higher densities stem from the much longer accumulation time-scale associated with a CM (typically months/years, see Appendix A in Townsend & Owocki 2005) than with a DM (typically hours, the dynamical time-scale). But a star such as HD 191612, with  $R_A \approx 2.7R_* \ll R_K \approx 55R_*$ , only has a DM contributing to the H $\alpha$  emission. So whereas rapidly rotating magnetic B-stars can indeed show substantial Balmer line emission, as observed in e.g.  $\sigma$  Ori E, the short accumulation time-scale of a DM requires the relatively high mass-loss rate of an O-star to produce observable H $\alpha$  emission in these slowly rotating stars.

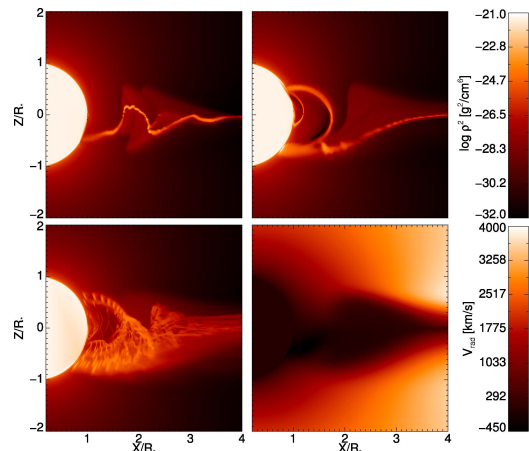


**Figure 2.** Contours of the density-squared for two different snapshots of the MHD wind simulation (upper panels), and of time-averaged density-squared (lower left) and radial velocity (lower right). Time averages are calculated from  $> 100$  snapshots taken well after the simulation’s initial state. The Alfvén radius is here located at  $r \approx 2.7R_*$  whereas the Kepler co-rotation radius is at  $r \approx 55R_*$ , i.e. outside the range of the plots.

### 3.2 Radiative transfer

To model the observed variation of Balmer emission, we compute synthetic H $\alpha$  flux profiles directly from the MHD simulations by solving the formal integral of radiative transfer in a 3-D cylindrical coordinate system  $(p, \xi, z')$ . This system is aligned toward the observer by rotating the stellar system  $(r, \theta, \phi)$  by an angle  $\alpha$  about its  $y$ -axis, so that  $\cos \alpha = \hat{z} \cdot \hat{z}'$ . The angle  $\alpha$  thus defines the observer’s viewing angle with respect to the magnetic pole. For given  $\beta$  and  $i$ , we have

$$\cos \alpha = \sin \beta \cos \Phi \sin i + \cos \beta \cos i, \quad (2)$$

which then readily gives the observer’s viewing angle as function of rotation phase  $\Phi$ . We note that even though the MHD models are 2-D, the radiative transfer must be performed in 3-D, as the axial symmetry is broken for any observer with  $|\cos \alpha| \neq 1$ .

The transfer equation is solved only in the wind, with a pre-specified photospheric profile  $P_\nu$  as a lower boundary condition, taken from NLTE model atmosphere calculations assuming negligible wind contamination. While not truly self-consistent, this procedure has been shown to be very accurate for H $\alpha$  line profile calculations in 1-D smooth (Puls et al. 1996) as well as multi-dimensional clumped (Sundqvist et al. 2011) O-star wind models without magnetic fields.

The monochromatic optical depth along a ray is

$$\tau_\nu = \int \chi_\nu dz', \quad (3)$$

where  $\chi_\nu$  is the frequency dependent opacity per unit length. The opacities are calculated assuming an optically thin continuum and occupation numbers for the H $\alpha$  atomic levels  $i$  given in terms of the NLTE departure coefficients  $b_i = n_i/n_*$ . Here  $n_*$  is the occupation number of level  $i$  in LTE with respect to the ground state of the next ionization state (e.g., Mihalas 1978). The line profile is a Gaussian of Doppler width  $\Delta\nu_D$ , set by the local wind electron temper-

ature  $T_e$ , and centered at zero co-moving frame frequency  $x_{\text{cmf}} = x_{\text{obs}} - \hat{z}' \cdot \vec{v}/v_\infty$ , where  $x = (\nu/\nu_0 - 1)c/v_\infty$ .

The emergent intensity for a given ray then is

$$I_\nu = P_\nu I_0 e^{-\tau_\nu^\infty} + \int_0^{\tau_\nu^\infty} S_\nu(\tau_\nu) e^{-\tau_\nu} d\tau_\nu, \quad (4)$$

where  $I_0$  is the stellar photospheric continuum intensity,  $S_\nu$  the NLTE line source function, and  $\tau_\nu^\infty$  the optical depth integrated over the complete ray.  $I_0$  is taken from FASTWIND model atmospheres for rays that intersect the stellar core and set to zero otherwise.  $S_\nu$  is fixed by the H $\alpha$  departure coefficients and the local wind electron temperature. The emergent flux is then, finally, obtained by integrating the emergent intensity over the projected stellar disc.

### 3.2.1 Electron temperatures and H $\alpha$ occupation numbers

As described, the H $\alpha$  synthesis problem requires estimates of  $T_e$  and the hydrogen departure coefficients. But the energy equation as treated in the MHD simulations described in Sect. 3.1 yields only a rough approximation of the wind temperature balance, with the local temperature artificially never allowed to drop below a certain floor value (on the order of the stellar effective temperature). In our H $\alpha$  calculations, we therefore estimate the wind temperature balance using the results of a spherically symmetric FASTWIND model, except in regions shock-heated to  $T_e > 10^5$  K, where we set the H $\alpha$  opacity and source function to zero.

To consistently calculate NLTE departure coefficients for a full multi-D MHD wind simulation is a daunting task, well beyond the scope of the present paper. However, for now we take advantage of the fact that hydrogen is almost fully ionized in typical O star winds. The H $\alpha$  line formation is then controlled by recombination, a thermal process, and the participating atomic levels are therefore very close to LTE with respect to ionized hydrogen. For HD 191612, FASTWIND calculations show deviations smaller than a factor of two, a typical number for most ‘normal’ O-star winds without strong magnetic fields (Puls et al. 1996; Sundqvist et al. 2011). As a first approximation then, we here take the simplest approach possible and assume LTE conditions, whereby  $b_i = 1$ .

## 4 H $\alpha$ VARIABILITY IN A DYNAMICAL MAGNETOSPHERE

We calculate an H $\alpha$  line profile for more than 100 snapshots of the 2-D MHD simulation of HD 191612. Fig. 3 shows that such profiles are highly variable, mimicking the wind’s dynamical nature. To obtain a mean profile at each phase, we average over such profiles for  $\sim 100$  randomly selected snapshots; this is intended to be a simple proxy for the real 3-D nature of the wind dynamics, effectively using the complex and non-linear variations in time in our 2-D simulation to mimic the expected variations in azimuth in a full 3-D model.<sup>1</sup> While approximate, this seems a reason-

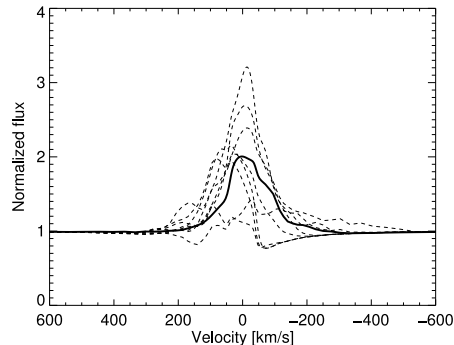


**Figure 3.** Synthetic H $\alpha$  profiles for 8 randomly selected snapshots during our simulation run (dashed lines), and a mean profile calculated from them (solid line).

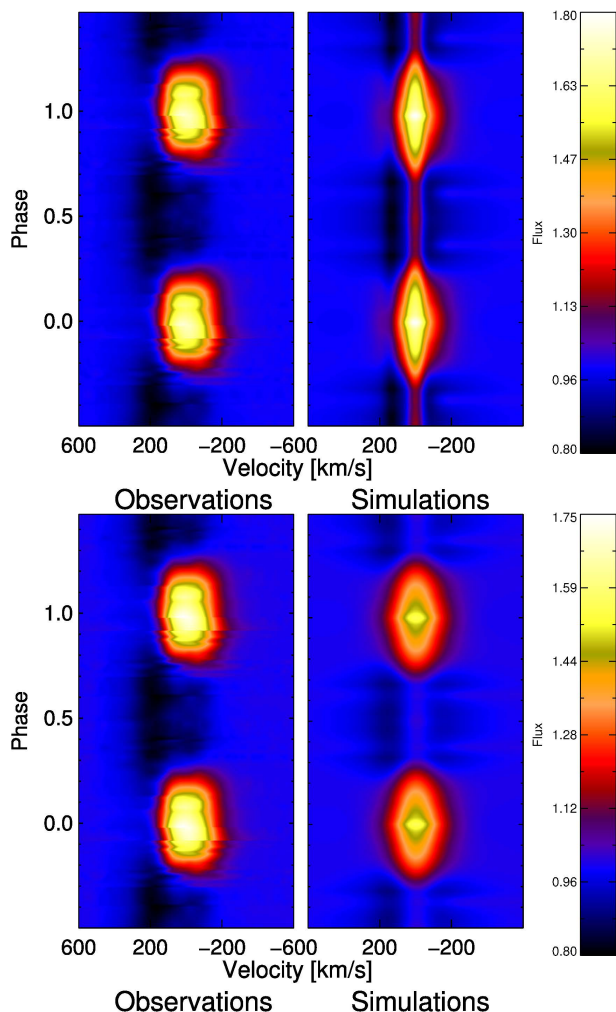


**Figure 4.** Observed (ephemeris from Howarth et al. 2007) and synthetic H $\alpha$  dynamic spectra, as functions of rotation phase and shown over two cycles. Synthetic spectra assume  $\beta = i = 50^\circ$  and are calculated as described in text. The model spectra in the lower panel have further been convolved with an isotropic ‘macro-turbulence’ of 100 km/s.

<sup>1</sup> For this type of line transfer, which often is optically thick, such post-averaging of the line profiles computed for many time snapshots is more realistic than the simple pre-processed, time-

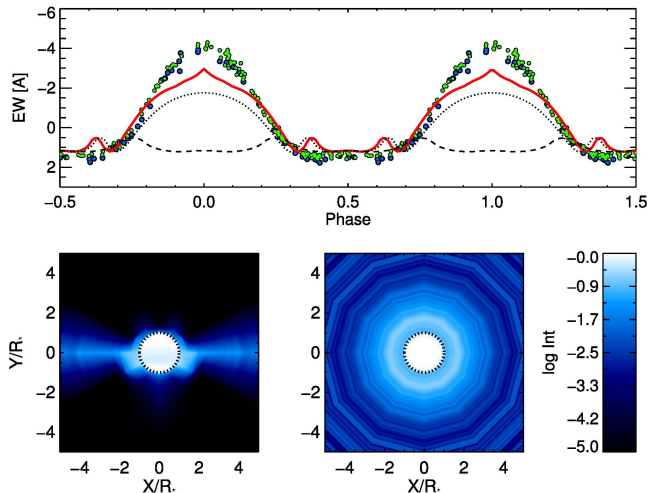


**Figure 5.** *Upper panel:* Observed (filled circles) and simulated H $\alpha$  equivalent widths as functions of rotation phase, for the three geometries  $i = \beta = 50^\circ$  (red, solid),  $i = 30^\circ$ ,  $\beta = 70^\circ$  (dotted), and  $i = 10^\circ$ ,  $\beta = 90^\circ$  (dashed). The blue filled circles represent the higher quality data points used in Fig. 4. *Lower panels:* Projected surface area contours of the normalized emergent intensity at line center, for observers located along the magnetic equator (left) and pole (right). Cartesian coordinate  $x'$  on the abscissa and  $y'$  on the ordinate.

able first approach to account for the limited lateral coherence or synchronization of an actual 3-D magnetized wind. Also, each phase is constructed by further averaging the two phases having equal  $\Phi$ 's when reversing the magnetic poles, to ensure the expected long-term north/south symmetry of our simulation. The procedures described above effectively smooth out most of the short-time variability of our simulation, in agreement with the observations (Howarth et al. 2007).

Fig. 4 compares observed and synthetic time-averaged dynamic H $\alpha$  spectra, plotted as functions of rotational phase assuming  $\beta = i = 50^\circ$ . This is consistent with the  $\beta + i = 95 \pm 10^\circ$  derived by Wade et al. (2011), but differs slightly from the  $i = 30^\circ$  adopted there (see further below). The observed general trends, with peak flux at phase 0 and an extended minimum around phase 0.5, are both well reproduced. The flux variations are caused by differences in the projected surface area of overdense H $\alpha$  emitting material as the observer changes viewing angle when the star rotates. Fig. 5 demonstrates this by plotting the H $\alpha$  emergent intensity (surface brightness) at line center for observers located along the axes of magnetic pole and equator. The figure clearly shows how the flux, which is just the integral of the intensity over this projected area, is much higher for the observer along the polar axis.

The large observed H $\alpha$  variability puts rather tight constraints on the system's geometry. The equivalent width curves in Fig. 5 directly refute very low values of  $i$ , but also show that the  $i = 30^\circ$ ,  $\beta = 70^\circ$  assigned as a tentative reference geometry by Wade et al. (2011) results in somewhat weaker variation than the  $\beta = i = 50^\circ$  adopted here.

averaged wind density used by Wade et al. (2011) to model polarized electron scattering, which is more nearly optically thin.

This is simply because, for a given sum  $i + \beta = 100^\circ$ , an observer at  $i = 30^\circ$  never looks closer to the magnetic pole than  $\alpha \approx 40^\circ$ , whereas for an observer at  $i = 50^\circ$ ,  $\alpha$  spans the entire range from pole to equator, and back again, in one rotation period, thus resulting in larger flux variations.

There are discrepancies, of course. Whilst the observed and simulated equivalent width curves qualitatively agree well, the simulated variation is quantitatively somewhat too low. These deviations could however be remedied if the DM were more concentrated, which would result in a larger surface brightness difference between pole and equator (Fig. 5). Such stronger wind confinement could occur from either a lower mass-loss rate or a stronger magnetic field, where the former choice seems more likely (due to clumping, Sect. 3.1), since the  $i = 50^\circ$  adopted here actually would result in a slightly reduced magnetic field strength as compared to that derived by Wade et al. (2011), who adopted  $i = 30^\circ$ . Another possibility is of course that these slight discrepancies simply are related to insufficient assumptions for the wind electron temperature structure and/or the hydrogen occupation numbers (Sect. 3.2.1).

In addition, the velocity dispersion in the models is too low, predicting narrower and sharper peaked profiles than observed (Fig. 4, upper panel). To illustrate this further, the lower panel of Fig. 4 displays the same line profiles as the upper panel, but now with the model profiles convolved with an isotropic Gaussian ‘macro-turbulence’ of 100 km/s. Inspection shows that the new profile shapes are significantly improved. We suspect that this required macro-turbulence is an artefact of missing wind dynamics, since, generally, the added degree of freedom in a 3-D simulation should result in larger velocity dispersion than in the 2-D models employed here. Though very challenging, 3-D MHD models are currently being developed by one of us (A. ud-Doula), and will be reported in a future paper. Such 3-D simulations will then also quantitatively test our simple approach here of averaging radiative transfer results for 2-D simulation snapshots to approximate the real 3-D dynamical wind structure.

Finally, notwithstanding the foregoing comments, there is surprisingly good overall agreement between the models and observations, which strongly supports that the DM model captures the key physics responsible for the H $\alpha$  variability.

## 5 DISCUSSION AND CONCLUSIONS

We have demonstrated that radiation magneto-hydrodynamical simulations of a confined wind, together with detailed radiative transfer modelling, reproduce well the distinct periodic H $\alpha$  emission observed in the magnetic O-star HD 191612. We interpret this within the context of a *dynamical magnetosphere* (DM), wherein the rotationally modulated spectral variations are results of a statistically overdense, low velocity wind region around the magnetic equator.

While applied here only to HD 191612, the DM model may also well describe optical Balmer line variability in other magnetic O stars with  $R_K > R_A$ , such as  $\theta^1$  Ori C and HD 148937 (Wade et al. 2006, 2011). Indeed, the narrow H $\alpha$  emission observed in HD 148937 suggests a line formation scenario in a DM, with the only significant difference

to HD 191612 then being the stellar and/or magnetic geometry (Wade et al. 2011), resulting in much smaller spectral variations for the former star. In future work, we intend to develop further this DM model and apply it to a broader sample of magnetic massive stars that show variable Balmer emission and are characterized by  $R_K > R_A$ .

## ACKNOWLEDGMENTS

G.A.W. acknowledges support from the Natural Science and Engineering Research Council of Canada. This work was supported in part by NASA ATP grant MANX11AC40G.

## REFERENCES

- Castor J. I., Abbott D. C., Klein R. I., 1975, *ApJ*, 195, 157
- Collier Cameron A., Jardine M., Wood K., Donati J.-F., 2003, in J. Arnaud & N. Meunier ed., *EAS Publications Series Vol. 9 of EAS Publications Series, Stellar prominences and coronal magnetic fields*. p. 217
- Donati J.-F., Howarth I. D., Bouret J.-C., Petit P., Catala C., Landstreet J., 2006, *MNRAS*, 365, L6
- Eibe M. T., Byrne P. B., Jeffries R. D., Gunn A. G., 1999, *A&A*, 341, 527
- Gagné M., Oksala M. E., Cohen D. H., Tonnesen S. K., ud-Doula A., Owocki S. P., Townsend R. H. D., MacFarlane J. J., 2005, *ApJ*, 628, 986
- Howarth I. D., Walborn N. R., Lennon D. J., Puls J., Nazé Y., Annuk K., Antokhin I., Bohlender D., Bond H. ., 2007, *MNRAS*, 381, 433
- Jardine M., van Ballegoijen A. A., 2005, *MNRAS*, 361, 1173
- Mihalas D., 1978, *Stellar atmospheres /2nd edition/*. San Francisco, W. H. Freeman and Co., 1978. 650 p.
- Owocki S. P., Castor J. I., Rybicki G. B., 1988, *ApJ*, 335, 914
- Petit V., Owocki S. P., Oksala M. E., the MiMeS Collaboration 2011, eprint ArXiv:1111.1238
- Puls J., Kudritzki R.-P., Herrero A., Pauldrach A. W. A., Haser S. M., Lennon D. J., Gabler R., Voels S. A., Vilchez J. M., Wachter S., Feldmeier A., 1996, *A&A*, 305, 171
- Puls J., Urbaneja M. A., Venero R., Repolust T., Springmann U., Jokuthy A., Mokiem M. R., 2005, *A&A*, 435, 669
- Sundqvist J. O., Owocki S. P., Puls J., 2011, eprint ArXiv:1110.0485
- Sundqvist J. O., Puls J., Feldmeier A., Owocki S. P., 2011, *A&A*, 528, A64+
- Townsend R. H. D., Owocki S. P., 2005, *MNRAS*, 357, 251
- Townsend R. H. D., Owocki S. P., Groote D., 2005, *ApJ*, 630, L81
- Townsend R. H. D., Owocki S. P., Ud-Doula A., 2007, *MNRAS*, 382, 139
- ud-Doula A., Owocki S. P., 2002, *ApJ*, 576, 413
- ud-Doula A., Owocki S. P., Townsend R. H. D., 2008, *MNRAS*, 385, 97
- Wade G. A., Fullerton A. W., Donati J.-F., Landstreet J. D., Petit P., Strasser S., 2006, *A&A*, 451, 195
- Wade G. A., Grunhut J., Graefener G., Howarth I. D., Martins F., Petit V., Vink J. S., Bagnulo S., Folsom C. P., Nazé Y., Walborn N. R., Townsend R. H. D., Evans C. J., the MiMeS Collaboration 2011, ArXiv e-prints
- Wade G. A., Howarth I. D., Townsend R. H. D., Grunhut J. H., Shultz M., Bouret J.-C., Fullerton A., Marcolino W., Martins F., Nazé Y., Ud Doula A., Walborn N. R., Donati J.-F., 2011, *MNRAS*, 416, 3160
- Walborn N. R., Howarth I. D., Herrero A., Lennon D. J., 2003, *ApJ*, 588, 1025